Shock Tube Modelling with L1d.

P. A. Jacobs
Research Report 13/98
Department of Mechanical Engineering
The University of Queensland.

November, 1998

Abstract

L1d is a computer program for the simulation of transient-flow facilities such as light-gas launchers and free-piston driven shock tunnels. The numerical modelling embodied within L1d is based on a quasi-one-dimensional Lagrangian description of the gas dynamics coupled with engineering correlations for viscous effects and point-mass dynamics for piston motion. This report describes the governing equations and a set of four example simulations:

- Sod's classic shock tube problem;
- an ideal gas gun;
- a fixed-driver shock tunnel; and
- a free-piston driven shock tunnel.

Contents

Nomenclature, Units

A	: duct area, m^2
a	: speed of sound, m/s
C_v	: specific heat at constant volume, $J/kg \cdot K$
C_p	: specific heat at constant pressure, $J/kg \cdot K$
D	: (effective) duct diameter, m
E	: total energy per unit mass $e + \frac{1}{2}u^2$, J/kg
e	: specific internal energy, J/kg
F_p	: piston friction force, N
F_{wall}	: wall shear force due to viscous effects, N
F_{loss}	: effective force due to pipe fitting losses, N
f	: Darcy-Weisbach friction factor / mass fraction
H	: total enthalpy, J/kg
h	: heat transfer coefficient, $J/s/m^2/K$
ix	: cell index (in computer code)
j	: cell index
K	: viscous loss coefficient
L	: length, m
M	: Mach number
MW	: molecular weight
m	: mass of fluid in a Lagrangian cell, kg
P, p	: pressure, Pa
Pr	: Prandtl number
Q	: source vector in the gas-dynamic equations
q	: heat transfer rate, J/s
R	: gas constant, $J/kg \cdot K$
R_0	: universal gas constant, $8314\ J/kg - mole \cdot K$
Re	: Reynolds number
r	: tube or duct radius, m
St	: Stanton number
T	: temperature, K
t	: time, s
U	: state vector in the gas-dynamic equations
$\overline{U}_L, \overline{U}_R$	: Riemann invariants
u	: local velocity, m/s
V	: piston velocity, m/s
v	: volume, m^3
$\dot{w}$	: work/unit time done by the wall shear stress, J/s
X	: piston position, m
x	: position, m
Z	: intermediate varaible for the Riemann solver

α : weighting parameter
β : stretching parameter
γ : ratio of specific heats
$\Delta\pm$: intermediate variable for interpolation
ϵ : absolute size of pipe roughness elements
λ : compression ratio for the free-piston driver
Λ : compressibility factor
π : 3.14159...
τ : wall shear stress, Pa
μ : viscosity, Pa.s; friction coefficient
Ω : recovery factor

Subscripts

aw : adiabatic wall condition
B : back of piston
F : front of piston
f : friction value
j : Lagrangian cell index
$j \pm \frac{1}{2}$: interface indices
$L,\ R$: left and right states for the Riemann solver
$loss$: pipe fitting value
p : piston
s : nozzle supply (stagnation) condition
/ species index
$wall$: wall condition

Superscripts

$*$: intermediate state for the Riemann solver
/ Eckert reference conditions
$\overline{(\cdots)}$: cell average

1 Introduction

In order to estimate the performance of a free-piston driven impulse facility, one must consider the both the dynamics of the piston and gases, the viscous effects (including heat transfer) simultaneously. Models which omit these effects require a number of facility-specific fudge factors which can be obtained accurately only after the construction and operation of the facility. This report describes the numerical modelling behind the computer code "l1d". L1d which is capable of simulating the (gas-dynamic) operation of a free-piston driven facility during the design process. It is closely related to other light-gas gun codes (see e.g. [1], [2], [3], [4], [5]) and borrows a number of ideas from some of them.

The principal features of l1d are:

- Quasi-one-dimensional formulation for the gas-dynamics. There is only one spatial coordinate but gradual variation of duct area is allowed.

- The ability to simulate several independent (or interacting) slugs of gas. Also, several pistons/projectiles and multiple diaphragms may be included. Coupling to the gas dynamics is via the boundary conditions of the gas slugs.

- A Lagrangian discretization of the gas slugs. This is done by dividing each gas slug into a set of control-masses (or gas particles) and following the positions of these particles.

- Nominal second-order accuracy in both space and time combined with a robust shock-capturing scheme. The use of a shock capturing scheme means that the same set of equations is used to compute the motion of the gas whether a shock is present or not. This simplifies the code (as shocks do not need to be explicitly identified or tracked) and is especially important in situations where shocks may form from the merger of finite compression waves and where multiple shocks and contact surfaces interact in a complicated manner. It also results in a smearing of the shocks over a couple of computational cells. However, in practice, this is not a problem as any smeared shocks can be sharpened by increasing the resolution of the discretization.

- Different gases may be simulated by including a suitable equation of state (which gives the pressure as a function of density and internal energy) and viscosity expression for each type of gas. Although only one type of gas may be included in any one gas slug, it may be a homogeneous mixture of other gases.

- Viscous effects are included using the standard engineering correlations for friction and heat transfer in pipe flow. Although these correlations are generally derived for steady

incompressible flow, they seem to perform adequately in the simulations where the flows are predominantly unsteady and are very compressible.

- The code is written in the C programming language and uses C's features of derived data structures and dynamic memory allocation to package the data in a straightforward manner. Thus, although several slugs of (different) gas may be required to simulate a particular facility, the basic code needs to know only how to simulate a generic gas slug. For each new configuration, the user simply supplies data for the number of gas slugs, pistons and diaphragms and then couples the components via boundary conditions.

The following section describes the numerical modelling that is built into the program and is essentially the same as in the original report [6]. However, example material presented in this report now concentrates on the simulation of shock tunnels. The companion report [7] is a hypertext document that describes the use of the program and provides links to the source code.

2 Governing Equations

The general procedure for modelling a specific facility (or system) is to divide the facility into its component parts such as the tube, pistons, diaphragms and volumes of gas (i.e. gas slugs). The description of each component is formulated separately and components allowed to interact through boundary conditions. The core of l1d is a time-stepping loop which first applies the specified boundary conditions and then advances the state of the entire system forward in time by a small increment (or time step). The generic components described in the following sections include a slug of compressible gas, a piston and a diaphragm.

2.1 Gas Dynamics

Each slug of gas is treated in a Lagrangian framework in which the slug is divided into a number of control-mass elements (or cells) moving in a variable-area duct. Flow in one dimension only is considered and any area changes in the tube area are assumed to be gradual. Although the boundary layer along the tube wall is not completely modelled in the formulation of the gas-dynamic equations, some of its effects are modelled in the momentum equation by the addition of a wall shear stress. These approximations are arguably the most troublesome part of the modelling process as they cannot be fixed later by simply increasing the resolution of the simulation.

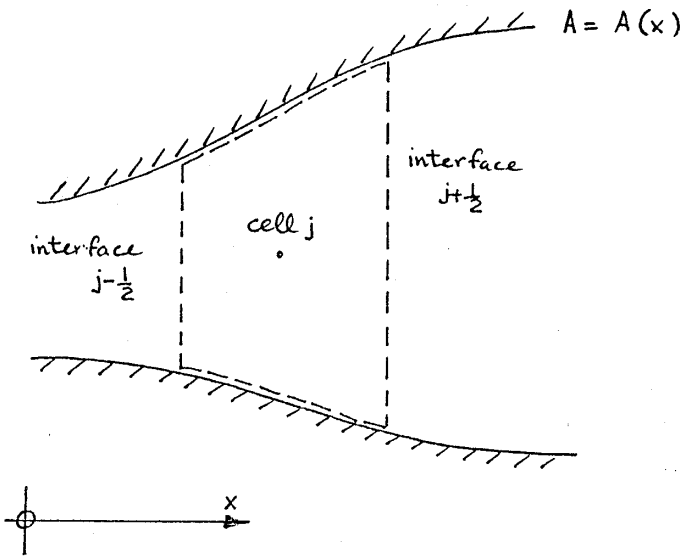

Figure 1: A typical control-mass or Lagrangian cell.

Figure 1 shows a typical control-mass cell (labelled j) with interfaces (labelled $j-\frac{1}{2}$ and $j+\frac{1}{2}$) to adjacent cells. At each interface, the Lagrangian description equates the local fluid velocity to the interface velocity as

$$\frac{dx_{j\pm\frac{1}{2}}}{dt} = u_{j\pm\frac{1}{2}} \quad , \tag{1}$$

where x is the position of the interface and u is the local gas velocity computed with a Riemann solver (to be described later).

The average density within the cell is given by

$$\overline{\rho_j} = \frac{m_j}{\overline{A_j}\left(x_{j+\frac{1}{2}} - x_{j-\frac{1}{2}}\right)} \quad , \tag{2}$$

where $\overline{(\cdots)}$ represents a cell average, A is the area of the duct and m_j is the (constant) mass of gas in cell j.

The rate of change of momentum in the cell is due to the pressure forces acting on the cell interfaces and viscous forces acting at the duct wall. It is given by

$$\frac{d}{dt} m_j \overline{u_j} = \left[P_{j-\frac{1}{2}} A_{j-\frac{1}{2}} - P_{j+\frac{1}{2}} A_{j+\frac{1}{2}} + \overline{P_j}\left(A_{j+\frac{1}{2}} - A_{j-\frac{1}{2}}\right) - \overline{F_{wall}} - \overline{F_{loss}}\right] \quad , \tag{3}$$

where F_{wall} is the shear friction force at the wall and F_{loss} is an effective body-force due to pipe-fitting losses, for example. Evaluation of these loss terms will be discussed in the viscous effects section 2.1.2.

The rate of change of energy within the cell is due to the work done at the cell interfaces plus the heat transferred through the duct wall. It is given by

$$\frac{d}{dt} m_j \overline{E_j} = \left[P_{j-\frac{1}{2}} A_{j-\frac{1}{2}} u_{j-\frac{1}{2}} - P_{j+\frac{1}{2}} A_{j+\frac{1}{2}} u_{j+\frac{1}{2}} + \overline{q_j} \right] \quad , \tag{4}$$

where $E = e + \frac{1}{2}u^2$ is the total specific energy of the gas and q is the rate of heat transfer into the cell. Evaluation of q will appear later in section 2.1.2. Note that there is no shear stress term in the total energy equation. This is because the energy removed from the kinetic energy component by the wall shear stress is deposited into the internal energy component of the gas near the wall and, since there is no transfer of mass from one cell to the next, the total energy of the cell is unchanged (by this mechanism).

2.1.1 Equations of State

The governing differential equations for the gas dynamics (i.e. equations (1), (3) and (4)) are completed by specifying the thermodynamic properties of the gas. For a perfect gas, the equation of state is

$$P = \rho \; R \; T \quad , \tag{5}$$

where R is the gas constant. If the gas is considered to be calorically perfect, the specific internal energy is proportional to the temperature and is given by

$$e = C_v \; T \quad , \tag{6}$$

where C_v is the specific heat capacity of the gas at constant volume. The equation of state may then be written as

$$P = \rho \; (\gamma - 1) \; e \quad , \tag{7}$$

and the speed of sound is given by

$$a^2 = \gamma \; R \; T = \gamma \; \frac{P}{\rho} = \gamma \; (\gamma - 1) \; e \quad . \tag{8}$$

The thermodynamic properties of a number of ideal gases are given in table 1 (see also table A.8 in [8]). For the Helium-Argon mixture, we use the perfect gas relations together with the effective thermodynamic properties

$$C_p = \sum_s f_s (C_p)_s \; , \quad C_v = \sum_s f_s (C_v)_s \; , \quad R = \sum_s f_s R_s \; , \quad \gamma = \frac{C_p}{C_v} \quad . \tag{9}$$

Here, the summation is over the two species.

Also, we consider air in chemical equilibrium and use the curve fits given in [9] to obtain P, T, a and γ as functions of ρ and e for temperatures up to 25000 K.

Gas	MW $(kg/kg-mole)$	R $(J/kg/K)$	γ	C_p $(J/kg/K)$	C_v $(J/kg/K)$
Air	28.97	287.0	1.400	1004.5	717.5
Hydrogen	2.016	4124.	1.409	14207.	10083.
Helium	4.006	2077.	1.667	5191.	3114.
Argon	39.948	208.1	1.667	520.1	312.
Nitrogen	28.013	296.8	1.400	1038.	742.
Oxygen	32.0	259.8	1.393	920.9	661.1
He,Ar mix	7.595	1094.	1.667	2735.	1641.

Table 1: Thermodynamic properties for some ideal gases. The He, Ar mix is 90% He and 10% Ar by volume.

2.1.2 Viscous Effects

The viscous shear force on a gas cell is given by

$$\overline{F_{wall}} = \tau_0 \ \pi \ \overline{D} \ (x_{j+\frac{1}{2}} - x_{j-\frac{1}{2}}) \quad , \tag{10}$$

where τ_0 is the local shear stress at the wall and $\overline{D}$ is the (average) effective diameter of the tube. Assuming a circular cross-section

$$\overline{D} = 2 \ (\overline{A}/\pi)^{1/2} \quad . \tag{11}$$

The wall shear stress is obtained from the Darcy formula for for steady incompressible flow (see e.g. [10, 11])

$$\tau_0 = \frac{-\rho \ f \ u \ |u|}{8} \quad , \tag{12}$$

where f is the Darcy-Weisbach friction factor. With minor changes, we follow [4] and use

$$\begin{aligned} f &= \frac{64}{\Lambda \ Re} \quad , \quad Re < 2000 \quad , \\ f &= \frac{0.032}{\Lambda} \left[\frac{Re}{2000}\right]^{0.3187} \quad , \quad 2000 \leq Re \leq 4000 \quad , \\ f &= \frac{1}{\Lambda} \left[1.14 - 2 \log_{10} \left(21.25 \ Re^{-0.9} + \frac{\epsilon}{D}\right)\right]^{-2} \quad , \quad Re > 4000 \quad , \end{aligned} \tag{13}$$

where the Re is the local Reynolds number based on tube diameter

$$Re = \frac{\rho^* \ D \ |u|}{\mu^*} \quad , \tag{14}$$

and ϵ is the absolute wall roughness. The explicit expression for f for the turbulent regime is taken from [12] and is within 1% of the well known Colebrook-White equation. For Reynolds

numbers up to 10^5 in shock-tube type flows, it is reasonable to assume a smooth wall and use

$$f = \frac{1}{\Lambda}\left[1.8\ \log_{10}(Re) - 1.5147\right]^{-2} \quad , \quad Re > 4000 \quad . \tag{15}$$

The properties μ^* and $\rho^* = \rho T/T^*$ are evaluated at the Eckert reference temperature (see e.g. [13] section 5.12)

$$T^* = T + 0.5(T_w - T) + 0.22(T_{aw} - T) \quad , \tag{16}$$

where T is the cell-average temperature, T_w is the specified wall temperature and

$$T_{aw} = \Lambda\ T \quad . \tag{17}$$

is the adiabatic wall temperature. Since, we are interested in flows which may have very high Mach numbers, a compressibility correction is applied via the the compressibility factor [14]

$$\Lambda = 1 + \frac{(\gamma - 1)}{2}\ \Omega\ M^2 \quad , \tag{18}$$

where M is the local Mach number and Ω is the recovery factor. Although the compressibility factor Λ in equations (13) and (15) was suggested for rough surfaces, we have used it to adjust the friction factor for all values of Re. For laminar flow (i.e. $Re < 2000$), the recovery factor is set to $\Omega = (Pr)^{1/2}$ while, for turbulent flow, $\Omega = (Pr)^{1/3}$.

Pressure losses due to sudden changes in tube cross-section are computed for each cell as

$$\overline{F_{loss}} = \frac{\Delta P_{loss}}{L_{loss}}\ \overline{A}\ \left(x_{j+\frac{1}{2}} - x_{j-\frac{1}{2}}\right) \quad , \tag{19}$$

where

$$\Delta P_{loss} = -K_L\ \frac{1}{2}\ \rho\ u\ |u| \quad , \tag{20}$$

and L_{loss} is the length of tube over which the pressure loss is distributed. Values of K_L/L_{loss} are stored along with the cross-sectional area for the tube. For a contraction and a diaphragm station, we use $K_L = 0.25$.

Heat transfer into a gas cell is given by ([13], section 5.12)

$$q = h\ \pi\ \overline{D}\ \left(x_{j+\frac{1}{2}} - x_{j-\frac{1}{2}}\right)\ (T_w - T_{aw}) \quad , \tag{21}$$

where the heat transfer coefficient is

$$h = \rho\ C_p\ |u|\ St \tag{22}$$

Gas	Pr	T_0 (K)	S_1 (K)	μ_0 $(\mu Pa.s)$
Air	0.72	273.1	110.4	16.77
Hydrogen	0.72	273.1	96.67	8.411
Helium	0.67	273.1	79.4	18.70
Argon	0.67	273.1	144.4	21.25
Nitrogen	0.72	273.1	106.67	16.63
Oxygen	0.72	273.1	138.89	19.19

Table 2: Viscous transport coefficients.

and the Stanton number is given by the modified Reynolds analogy for turbulent flow in pipes ([13], section 6.2)

$$St = \frac{f}{8}\ Pr^{-2/3} \quad . \tag{23}$$

The dynamic viscosity of the gas is given by the Sutherland expression

$$\mu = \mu_0 \left(\frac{T}{T_0}\right)^{3/2} \left(\frac{T_0 + S_1}{T + S_1}\right) \quad , \tag{24}$$

where values of μ_0, T_0 and S_1 are given for a number of gases in table 2. The viscosities for mixtures of gases is obtained from Wilke's [15] expression

$$\mu_{mix} = \sum_{s=1}^{N} \frac{f_s\ \mu_s}{MW_s\ \Phi_s} \quad , \tag{25}$$

where

$$\Phi_s = \sum_{s'=1}^{N} \frac{f_{s'}}{MW_{s'}} \left[1 + \left(\frac{\mu_s}{\mu_{s'}}\right)^{1/2} \left(\frac{MW_{s'}}{MW_s}\right)^{1/4}\right]^2 \left[8\left(1 + \frac{MW_s}{MW_{s'}}\right)\right]^{-1/2} \quad . \tag{26}$$

Following [4], the Prandtl number is given approximately as

$$Pr = \frac{20\gamma}{39\gamma - 15} \quad . \tag{27}$$

2.1.3 Data Structures

Data for each slug of gas is stored in a data structure (called "slug_data") which contains an array of "L_cell" structures (one element for each Lagrangian cell) and other data such as boundary flags and time step information. Each Lagrangian cell (L_cell) structure contains the location of the cell midpoint, the location of the interface to the right, the mass contained by the cell, a cell average of the local flow state, and time derivatives of the state variables. Full details may be obtained from the header file "lid.h".

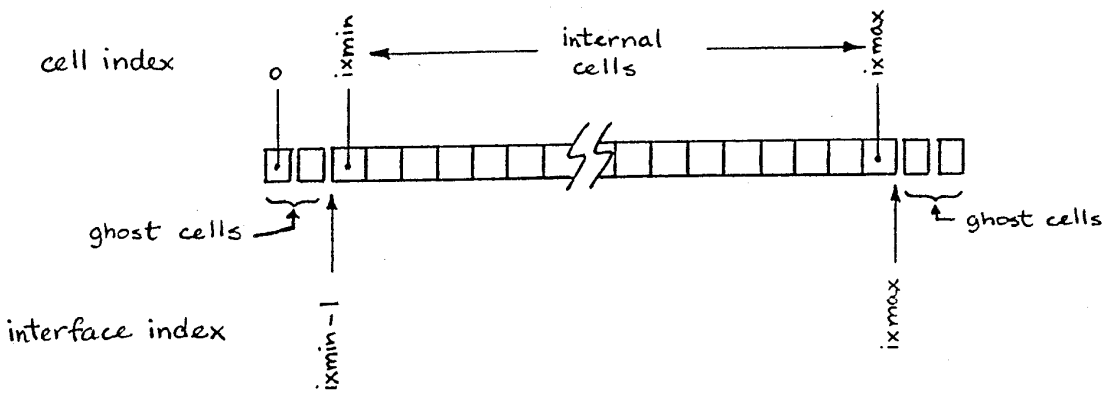

Figure 2: Data storage for a single slug of gas. The indexing for the cells is shown above the array while the indexing scheme for the interfaces is shown below.

Figure 2 shows the indexing arrangement for the cells within each slug data structure. The array consists of both internal cells ($ixmin \leq ix \leq ixmax$) and ghost cells at each end ($ixmin-2,\ ixmin-1,\ ixmax+1,\ ixmax+2$). The ghost cells lie outside the physical gas slug and contain data used in the application of the boundary conditions.

2.1.4 Internal-Interface Pressures and Velocities

The pressures and velocities used in equations (3) and (4) are obtained by first interpolating the flow state (consisting of a set of values for $\rho,\ u,\ v,\ e,\ P,\ a$) from the cell centres to either side of each interface at the start of the time step and then applying a Riemann solver to estimate the flow states at the interfaces during the time step.

The state of the flow either side of each interface "L" and "R" is interpolated (or reconstructed) from the set of cell averaged states by assuming a linear variation of the variables within cells. This interpolation is performed separately for each primary variable. For example, the density either side of interface $(j+\frac{1}{2})$ is obtained by a nonlinear interpolation (or reconstruction) using the expressions

$$\begin{aligned} \rho_L &= \rho_j + (x_{j+\frac{1}{2}} - x_j)\ \text{MINMOD}((\Delta-)_j, (\Delta+)_j)\ , \\ \rho_R &= \rho_{j+1} + (x_{j+\frac{1}{2}} - x_{j+1})\ \text{MINMOD}((\Delta-)_{j+1}, (\Delta+)_{j+1})\ , \end{aligned} \tag{28}$$

where

$$(\Delta-)_j = \frac{\rho_j - \rho_{j-1}}{x_j - x_{j-1}}\ ,$$

$$(\Delta+)_j \;=\; \frac{\rho_{j+1}-\rho_j}{x_{j+1}-x_j}\;, \tag{29}$$

represent two possible estimates of the slope of the density for cell j and x_{j-1}, x_j, x_{j+1} are the midpoints of the cells $j-1$, j and $j+1$ respectively. The MINMOD limiter function selects the slope with the minimum magnitude if both slopes have the same sign and returns zero otherwise (see e.g. [16]).

Interpolation for the other variables is done similarly. To make the code more robust, the conditions $\rho_L, \rho_R \geq \rho_{MIN}$ and $e_L, e_R \geq e_{MIN}$ are imposed after interpolation but before the application of the Riemann solver. Details of the Riemann solver are already available in [17], but for completeness and because the solver is related to the implementation of the specified-velocity boundary condition, a complete description is included here.

The Riemann solver used here is a 2-stage approximate solver in which the first stage computes the intermediate pressure and velocity assuming isentropic wave interaction. A second stage, based on the strong-shock relations, may be invoked to improve the first-stage estimate if the pressure jumps across either wave are sufficiently large. In practice, this modification has been required only in extreme conditions [17]. If stage 2 (strong shock modification) is not invoked, the solver is much like Osher's approximate Riemann solver [18].

STAGE 1: The first stage of the Riemann solver assumes that a spatially constant left state (subscript L) and right state (subscript R) interact through a pair of finite-amplitude (and isentropic) compression or rarefaction waves. Perfect gas relations ([19] cited in [20]) are used to obtain the intermediate states (L^*, R^*) in the gas after the passage of left-moving and right-moving waves, respectively. The expressions implemented in the code are

$$P_L^* = P_R^* = P^* = P_L \left[\frac{(\gamma-1)(\overline{U}_L - \overline{U}_R)}{2a_L(1+Z)} \right]^{2\gamma/(\gamma-1)}\;, \tag{30}$$

and

$$u_L^* = u_R^* = u^* = \frac{\overline{U}_L Z + \overline{U}_R}{1+Z}\,, \tag{31}$$

where the Riemann invariants are

$$\begin{aligned} \overline{U}_L &= u_L + \frac{2a_L}{\gamma-1}\;, \text{ and} \\ \overline{U}_R &= u_R - \frac{2a_R}{\gamma-1}\;, \end{aligned} \tag{32}$$

and the intermediate variable Z is given by

$$Z = \frac{a_R}{a_L}\left(\frac{P_L}{P_R}\right)^{(\gamma-1)/(2\gamma)}\;. \tag{33}$$

In the exceptional situation of $(\overline{U}_L - \overline{U}_R) < 0$, we assume that a (near) vacuum has formed at the cell interface and set all of the interface quantities to minimum values.

STAGE 2: If the pressure jump across either wave is large (say, a factor of 10), then the guess for the intermediate pressure is modified using the strong shock relations.

If $P^* > 10\ P_L$ and $P^* > 10\ P_R$ then both waves are taken to be strong shock waves and the intermediate pressure and velocity can be determined directly as

$$P^* = \frac{\gamma+1}{2}\rho_L\left[\frac{\sqrt{\rho_R}}{\sqrt{\rho_R}+\sqrt{\rho_L}}(u_L - u_R)\right]^2 \quad , \tag{34}$$

and

$$u^* = \frac{\sqrt{\rho_L}\ u_L + \sqrt{\rho_R}\ u_R}{\sqrt{\rho_R}+\sqrt{\rho_L}} \quad . \tag{35}$$

If P^* is greater than P_L or P_R (but not both), the stage-1 estimate for P^* can be improved with two Newton-Raphson steps of the form

$$P^*_{n+1} = P^*_n - F_n\left(\frac{dF_n}{dP^*}\right)^{-1} \quad , \tag{36}$$

where

$$F_n = u^*_L(P^*_n) - u^*_R(P^*_n) \quad , \tag{37}$$

and

$$u^*_L = \begin{cases} \overline{U}_L - \frac{2a_L}{\gamma-1}\left(\frac{P^*}{P_L}\right)^{\frac{\gamma-1}{2\gamma}} & , \quad P^* \le 10\ P_L \quad , \\ u_L - \left(\frac{2P^*}{\rho_L(\gamma+1)}\right)^{1/2} & , \quad P^* > 10\ P_L \quad , \end{cases} \tag{38}$$

$$u^*_R = \begin{cases} \overline{U}_R + \frac{2a_R}{\gamma-1}\left(\frac{P^*}{P_R}\right)^{\frac{\gamma-1}{2\gamma}} & , \quad P^* \le 10\ P_R \quad , \\ u_R + \left(\frac{2P^*}{\rho_R(\gamma+1)}\right)^{1/2} & , \quad P^* > 10\ P_R \quad . \end{cases} \tag{39}$$

During the update, we ensure that $P^* \ge P_{MIN}$ where P_{MIN} is some small value. After updating P^*, the intermediate velocity is evaluated using the relevant strong-shock relation from (38) or (39).

The pressure and velocity at each interface may now be substituted back into equations (1), (3) and (4) to give the motion of the cell interfaces and the rate of change of momentum and energy within the cells.

2.1.5 Boundary Conditions

Before interpolation, the inviscid boundary conditions are applied by setting up two layers of ghost cells along each of the boundaries. This is shown schematically in Fig. 3. For a

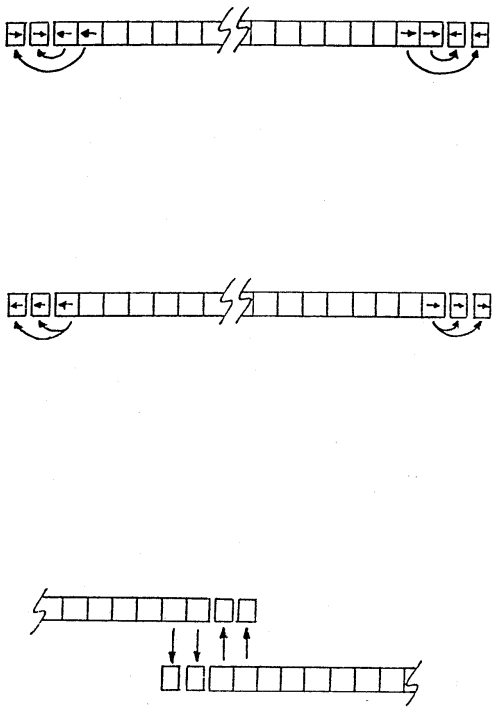

Figure 3: Applying boundary conditions via ghost cells: (a) reflecting end condition; (b) supersonic outflow; (c) gas-gas interface (or direct exchange of data).

supersonic inflow boundary, all of the ghost-cell quantities are specified as fixed while, for a supersonic outflow boundary, the ghost-cell quantities are extrapolated from active cells just inside the boundary. Solid-wall (i.e. reflective) boundary conditions are applied by setting all of the scalar quantities in the ghost cells equal to those in the active cells adjacent to the boundary but setting the ghost-cell velocities to the negative of the velocities in the active cells. Where two gas slugs interact, data between the two end-cells of the first slug and the corresponding ghost-cells of the second slug are exchanged as shown in Fig. 3.

Where the gas interacts with a piston (or end wall), the boundary-interface velocity u^* is specified. The interface pressure may then be determined from the isentropic relations which, for a right-end boundary, give

$$P^* = \left[(\overline{U}_L - u^*) \frac{(\gamma - 1)}{2\gamma^{1/2}} \left(\frac{\rho_L}{P_L^{1/\gamma}} \right)^{1/2} \right]^{2\gamma/(\gamma-1)} \quad . \tag{40}$$

Similarly, the interface pressure at a left-end boundary is given as

$$P^* = \left[(u^* - \overline{U}_R) \frac{(\gamma - 1)}{2\gamma^{1/2}} \left(\frac{\rho_R}{P_R^{1/\gamma}} \right)^{1/2} \right]^{2\gamma/(\gamma-1)} \quad . \tag{41}$$

2.2 Piston Dynamics

Each piston is assumed to have fixed mass (m_p), length (L_p) and frontal area (A_p). The piston state is given by a flag indicating whether the piston is constrained, its centroid position (x_p) and its velocity (V_p). The governing differential equations are

$$\begin{aligned} \frac{d}{dt} x_p &= V_p \quad , \\ \frac{d}{dt} V_p &= \frac{1}{m_p} [A_p (P_B - P_F) + F_f] \quad , \end{aligned} \tag{42}$$

where P_B and P_F are the pressures on the "back" and "front" piston faces respectively and F_f is the total frictional force. Refer to Fig. 4 for the general arrangement. If the piston is initially restrained, a specified value of back-face pressure (P_B) must be exceeded before the piston is released.

For the simulation of the T4 facility, the frictional force is assumed to be due to the "chevron" seal near the front face of the piston. The maximum magnitude of the frictional force is

$$|F_f|_{max} = \mu_f A_{seal} P_F \quad , \tag{43}$$

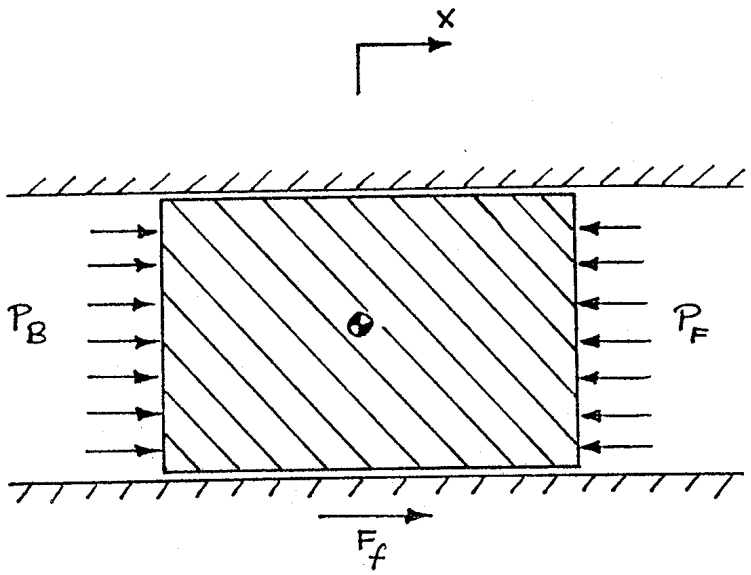

Figure 4: Schematic diagram showing the pressure forces on a piston.

where μ_f is the coefficient of friction of the seal material on the tube wall (taken to be 0.2) and A_{seal} is the effective frontal-area of the seal. The actual value of F_f used in equation (42) is

$$F_f = \begin{cases} -sign(V_p)\ |F_f|_{max} & \text{if } (|V_p| \geq V_{tol} \text{ or } |A_p(P_B - P_F)| \geq |F_f|_{max}) \\ -A_p(P_B - P_F) & \text{if } (|V_p| < V_{tol} \text{ and } |A_p(P_B - P_F)| < |F_f|_{max}) \end{cases} \tag{44}$$

where the velocity tolerance is $V_{tol} = 10^{-6}\ m/s$.

2.3 Diaphragms

Diaphragms are implemented as a flag for the status of the diaphragm (intact or burst) and a burst pressure. Note that the burst pressure is a "dynamic" burst pressure which may be significantly higher than the burst pressure obtained in hydrostatic rupture tests [21]. The effect of the diaphragm is coded directly into l1d.x as a change in boundary conditions selected by the diaphragm's status flag. For example, two gas slugs initially separated by a diaphragm will have reflective boundary conditions applied at the diaphragm station. On rupture, the applied boundary conditions will be changed to a data-exchange condition.

2.4 Time Stepping

The state quantities for both pistons and gas slugs are advanced from time level n to time level $n+1$ with the predictor-corrector scheme

$$\begin{aligned} \Delta U^{(1)} &= \Delta t \, \frac{dU^{(n)}}{dt} \quad , \\ U^{(1)} &= U^{(n)} + \Delta U^{(1)} \quad , \\ \Delta U^{(2)} &= \Delta t \, \frac{dU^{(1)}}{dt} \quad , \\ U^{(n+1)} &= U^{(1)} + \frac{1}{2}\left(\Delta U^{(2)} - \Delta U^{(1)}\right) \quad , \end{aligned} \tag{45}$$

where the superscripts (1) and (2) indicate intermediate results and $(\frac{dU}{dt})$ includes the rate of change of interface positions, cell momentum, cell energy, piston velocity and piston position. If a first-order scheme is desired, only the first stage is used and $U^{(n+1)} = U^{(1)}$. Although first-order time-stepping requires fewer operations than second-order time-stepping, it is also less robust.

To maintain stability, the time step is restricted to

$$\Delta t \leq \Delta t_{allowed} = CFL \; \Delta t_{signal} \quad , \tag{46}$$

where $\Delta t_{allowed}$ is the smallest value for all cells (and all gas slugs) and CFL is the specified Courant-Friedrichs-Lewy number. It is normally restricted to $CFL \leq 0.5$ in the simulations discussed later. For each cell, the inviscid signal time is approximated as

$$\Delta t_{signal} = \frac{\Delta x}{|u| + a} \quad . \tag{47}$$

3 Test Cases

3.1 Sod's Shock Tube Problem

The first test case is the so-called one-dimensional shock tube problem used by Sod [22]. The duct has a constant diameter of $D = 0.01$ m and extends from $x = 0$ to $x = 1.0$ m. Two slugs of calorically perfect air with $\gamma = 1.4$ (labelled 0 and 1) are each discretized into 50 cells. Reflecting boundary conditions are applied at each end of the duct and an exchange boundary condition is applied where the gas slugs meet in the middle of the duct. Viscous effects are omitted. For slug[0], $x \leq 0.5$m, the initial state is

$$\rho = 1.0 \text{ kg/m}^3, \quad P = 10^5 \text{ Pa}, \quad u = 0, \quad T = 348.4 \text{ K}, \quad e = 2.5 \times 10^5 \text{ J/kg} \cdot \text{K},$$

while, for slug[1], $x > 0.5m$, it is

$$\rho = 0.125 \text{ kg/m}^3, \quad P = 10^4 \text{ Pa}, \quad u = 0, \quad T = 278.7 \text{ K}, \quad e = 2.0 \times 10^5 \text{ J/kg} \cdot \text{K}.$$

The input parameter file is shown below. Boundary conditions are that the left-end of slug [0] is fixed, the right-end of slug [0] exchanges data with the left-end of slug [1], and the right-end of slug [1] is fixed.

```
Sod's ideal shock tube, 19-Jan-99
0                   test_case
2 0 0               nslug, npiston, ndiaphragm
0.6e-3   5000       max_time, max_steps
1.0e-6   0.50       dt_init, CFL
2 2                 Xorder, Torder
10.0e-6  5.0e-6     dt_plot, dt_his
1                   hnloc
0.70                hcell[0]: location is near upstream wall
tube definition follows:
100  1              n, nseg
 0.00  0.010  1     xb[0], Diamb[0], linear[0]
 1.00  0.010  1       [1]
0                   nKL
296.0  0            Tnominal, nT
slug 0: perfect air driver
100 0 1 1.1         nnx, to_end_1, to_end_2, strength
0 0                 viscous, adiabatic
V  0.0              left boundary : velocity (fixed wall)
S  1  L             right boundary: another slug
1                   hn_cell
1                   hx_cell: the left-most cell
0.0 0.5 0 1.0e5 0.0 348.4 Initial: x1, x2, gas, p, u, T
slug 1: perfect air driven gas
100 0 0 0.0         nnx, to_end_1, to_end_2, strength
```

```
0 0                  viscous, adiabatic
S  0  R              left boundary : another slug
V  0.0               right boundary: velocity (fixed wall)
1                    hn_cell
1                    hx_cell: the left-most cell
0.5 1.0 0 1.0e4 0.0 278.7 Initial: x1, x2, gas, p, u, T
```

At $t = 0$, the hypothetical diaphragm (initially separating the two slugs) is removed and the inviscid equations are integrated in time to $t \simeq 0.60 \times 10^{-3} s$ with $CFL \simeq 0.5$. The resulting flow state is shown in Fig. 5. Comparison with the exact solution (see e.g. [23]) is reasonably good. The shock is captured in three or four cells and has the correct speed. As expected for a Lagrangian scheme, the contact discontinuity is sharp but has a small glitch possibly due to the starting error ([24]). The edges of the expansion fan show some smearing but can be sharpened by using a finer initial discretization.

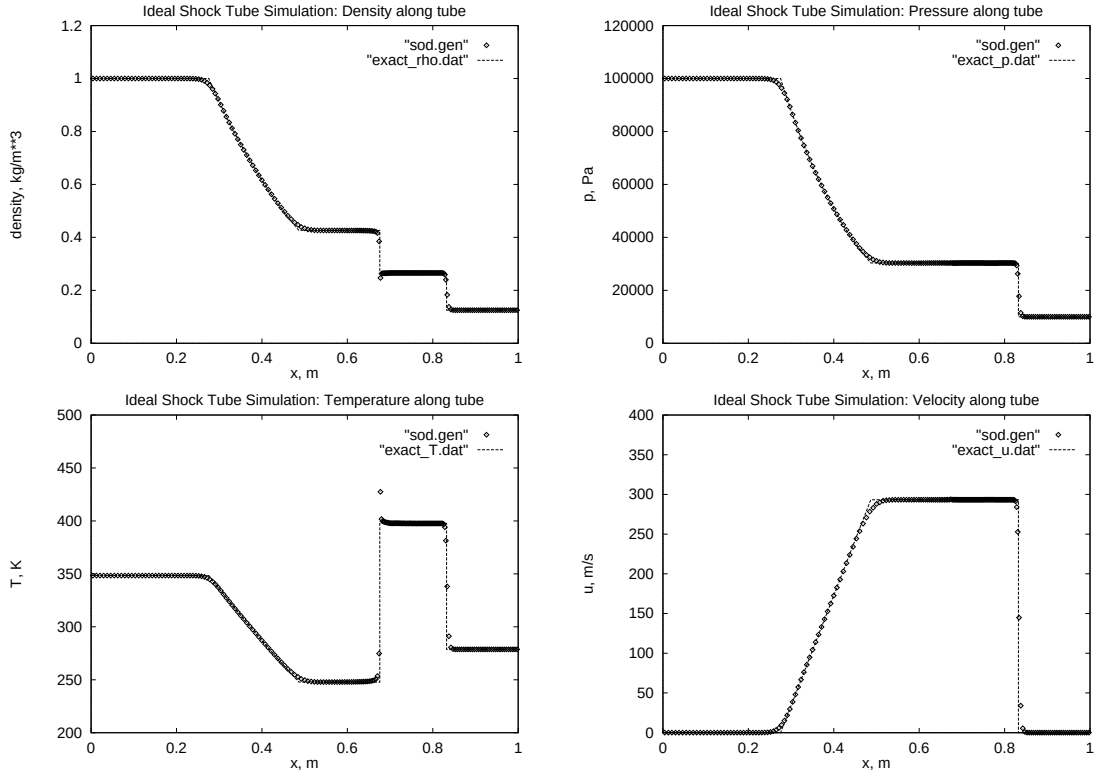

Figure 5: Flow state for the Sod shock tube problem, $t = 0.6\ ms$.

Figure 6 shows a space-time diagram consisting of contours of density superimposed on a grid of the cell centres shown at at regular time intervals. Both the shock and the expansion fan are identified by straight contours and the contact surface is identified as the gap between the two slugs of gas. (Note that the contact appears as a gap because we are plotting the

data at cell centres.) The evolving solution is therefore self-similar (except for some small resolution-related wiggles).

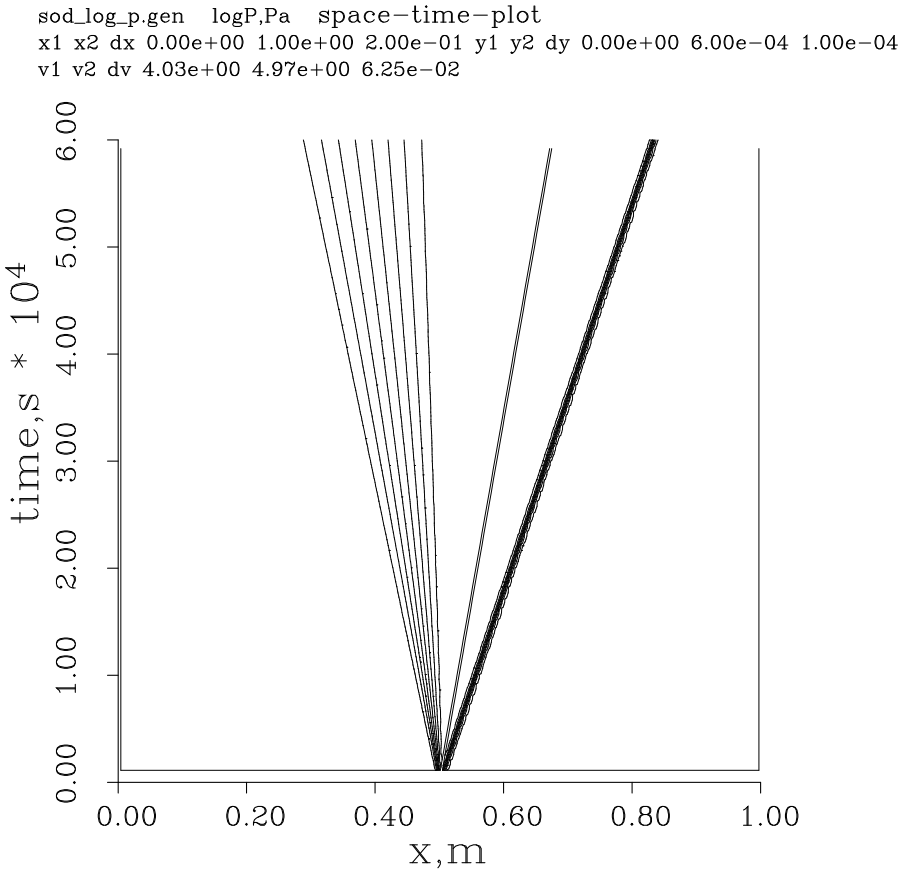

Figure 6: Space-time diagram for the Sod shock tube problem.

Of the test cases discussed here, this test case is simplest and requires the least memory and processing time. It should require only a few seconds of CPU time.

3.2 Projectile-In-Tube

This case is used to demonstrate the coupling of the piston dynamics with the gas dynamics. It simulates the motion of a light projectile being driven by a finite-length reservoir. The parameter file is shown below.

```
Ideal piston and gas slug 11-Apr-98, 19-Jan-99
0                    test_case
1 1 0                nslug, npiston, ndiaphragm
50.0e-3  5000        max_time, max_steps
1.0e-6   0.50        dt_init, CFL
2 2                  Xorder, Torder
```

```
0.2e-3  20.0e-6     dt_plot, dt_his
1                   hnloc
-3.99               hcell[0]: location is near upstream wall
tube definition follows:
100  1              n, nseg
-6.00  0.010  1     xb[0], Diamb[0], linear[0]
 6.00  0.010  1       [1]
0                   nKL
296.0  0            Tnominal, nT
piston [0] is ideal
0                       type_of_piston
0.001  0.010  0.010     mass, diam, length
0.0e6   0               p_restrain, is_restrain
20.00   0               x_buffer, hit_buffer
0       0               with_brakes, brakes_on
0       R               left_slug_id, left_slug_end_id
-1      R               right_slug_id, right_slug_end_id
0.005 0.0               x0, V0
slug 0: perfect air driver
100 0 1 1.1         nnx, to_end_1, to_end_2, strength
0 0                 viscous, adiabatic
V  0.0              left boundary : velocity (fixed wall)
P  0                right boundary: piston
1                   hn_cell
100                 hx_cell: the cell pushing against the piston
-4.0 -0.005 0 1.0e5 0.0 348.4 Initial: x1, x2, gas, p, u, T
```

The duct has a constant diameter of 10 mm and extends from $x = -6$m to $x = 6$m. The reservoir gas (slug[0]: $-4.0 \leq x \leq -0.005$ m; 100 nonuniformily spaced cells) is ideal air (gas type 0) with

$$\rho = 1.0 \text{ kg/m}^3, \quad P = 1.0 \times 10^5 \text{ Pa}, \quad u = 0, \quad T = 348.4 \text{ K}, \quad e = 2.5 \times 10^5 \text{ J/kg}.$$

There is no gas in front of the piston. The piston has the same area as the tube, a length of 0.01 m and a mass, $m_p = 0.001$ kg. Boundary conditions for the gas slug are that the left-end has zero velocity and that the right-end is coupled to the left-end of the piston.

The simulation starts at $t = 0$ with the release of the projectile. As shown in Figure 7, the projectile accelerates along the tube and allows the driver gas to expand behind it. Note that, in the plot, the piston is located on the right-hand end of the gas slug. An expansion can be seen propagating to the left into the quiescent driver gas and (at $t \approx 10$ ms) reflecting off the end of the tube. At $t \approx 23$ ms the reflected expansion has reached the piston and further decreases the pressure of the gas driving the piston (see Figure 8).

Figures 10 and 9 compare the computed position and velocity with that obtained from the theory in [25]. The theory assumes an infinitely long driver and a vacuum in front of the

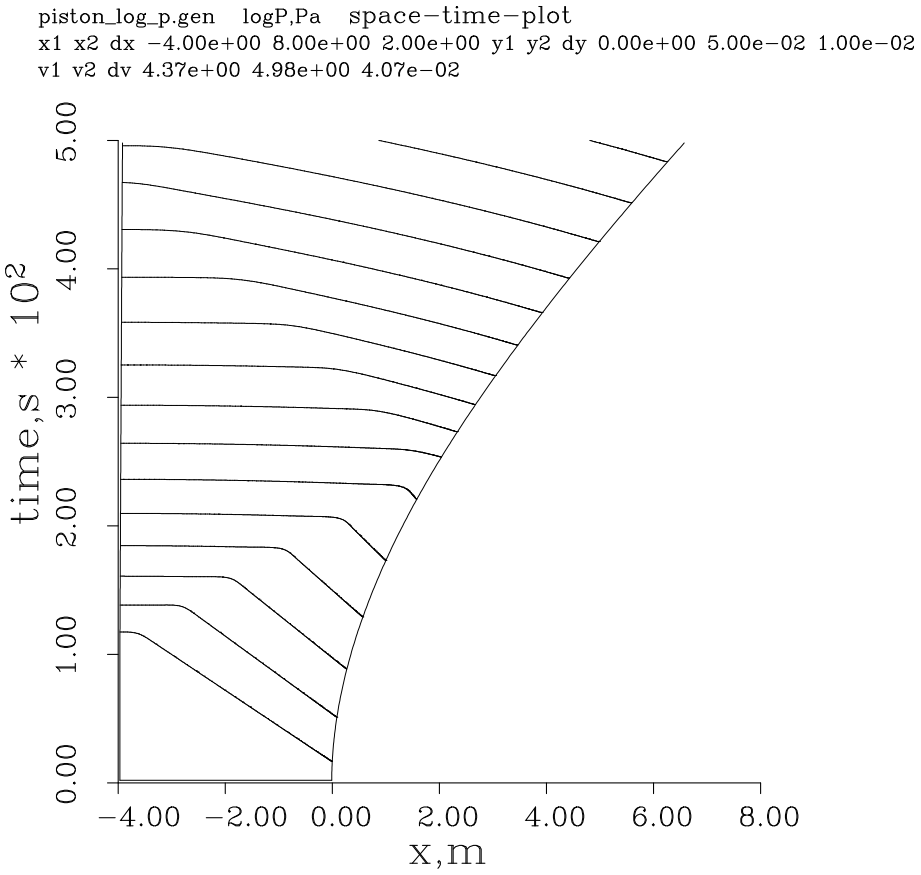

Figure 7: Space-time diagram for the projectile-in-tube problem.

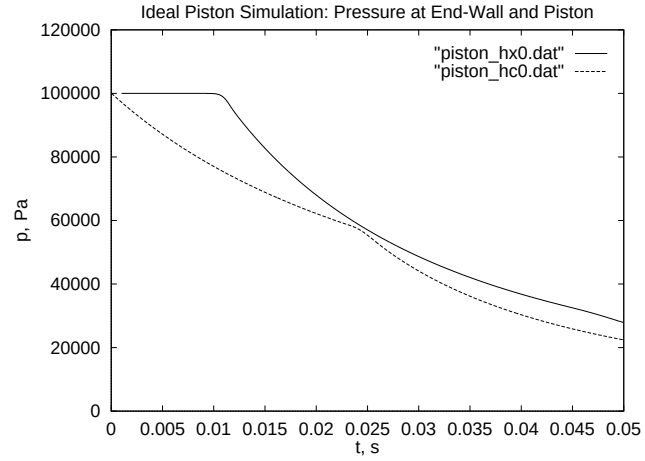

Figure 8: Pressure at the upstream end of the driver (solid line) and against the upstream-face of the piston (dashed line).

projectile. As expected, the comparison is fairly good up until the time that the expansion reaches the projectile. In terms of a nondimensional time, the projectile velocity and position are given by [25]

$$\begin{aligned} \overline{x} &= \frac{2}{\gamma-1}\left\{1+\overline{t}-\left[1+\left(\frac{\gamma+1}{2}\right)\overline{t}\right]^{2/(\gamma+1)}\right\} \quad , \\ \overline{V} &= \frac{2}{\gamma-1}\left\{1-\left[1+\left(\frac{\gamma+1}{2}\right)\overline{t}\right]^{-(\gamma-1)/(\gamma+1)}\right\} \quad , \end{aligned} \tag{48}$$

where the nondimensional quantities of time, position and velocity are

$$\overline{t} = \frac{P_R A t}{m_p a_R} \ , \quad \overline{x} = \frac{P_R A x}{m_p a_R^2} \ , \quad \overline{V} = \frac{V}{a_R} \ . \tag{49}$$

Here $a_R = 374.17\ m/s$ and $P_R = 1.0 \times 10^5$ are the initial values for the speed of sound and the pressure of the reservoir gas.

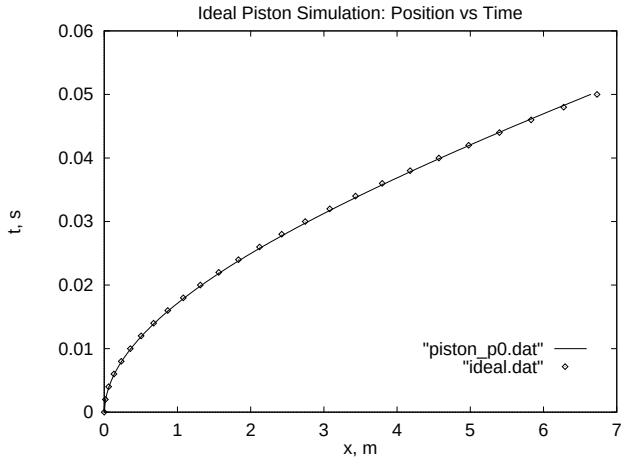

Figure 9: Piston position for the projectile-in-tube problem: solid line denotes the computed result; small circles denote the theoretical result for a long driver.

It has been found that the accuracy of expansion fan simulations is sensitive to grid resolution and better accuracy can be obtained by clustering cells in regions where expansion fans will develop. The clustering is done prior to the simulation (i.e. in l_prep.c) by distributing the cells according to the grid-stretching functions of Roberts [26] (see also [27]). For this simulation, the computational cells have been set up so that they are clustered close to the projectile. In the parameter file, the value of *to_end_2* is 1 and the *strength* is set to 1.1. Stronger clustering can be produced by allowing *strength* to approach a value a little larger than 1.0.

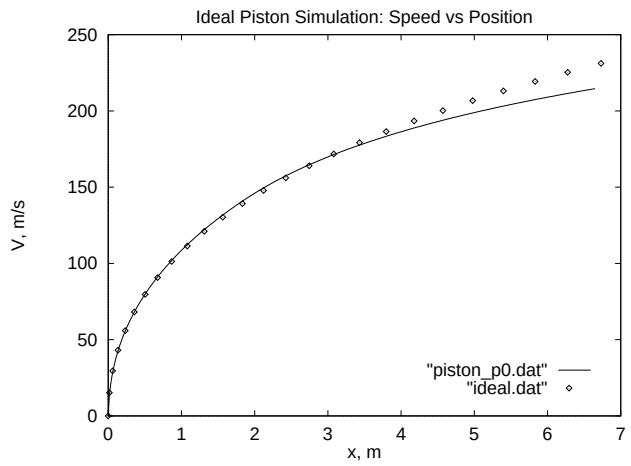

Figure 10: Velocity as a function of displacement for the projectile-in-tube problem: solid line denotes the computed result; small circles denote the theoretical result for a long driver.

3.3 Drummond Shock Tunnel

Hardware reports [28, 29].

```
Drummond tunnel M4 nozzle P4 = 3.25MPa N2, P1 = 30kPa N2. 20-Jan-99
27                  test_case, Mach 4 nozzle attached
3 0 1               nslug, npiston, ndiaphragm
8.0e-3   250000     max_time, max_steps
0.5e-6   0.25       dt_init, CFL
2 2                 Xorder, Torder
30.0e-6  2.0e-6     dt_plot, dt_his
5                   hnloc
-0.295              hxloc[0], heat flux gauge
-0.078              hxloc[1], pressure transducer
 0.000              hxloc[2], joint at nozzle block
 0.090                   [3]  mid-point of nozzle throat
 0.265                   [4], nozzle exit plane
tube definition follows:
4000  7             n, nseg
-3.785  0.0585    0 xb[0], Diamb[0], linear[0]
-3.035  0.0585    0   [1]
-3.015  0.0620    0   [2]
 0.000  0.0620    0   [3]
 0.043  0.0620    0   [4]
 0.080  0.0220    0   [5]
 0.100  0.0220    1   [6]   Parallel section of throat
 0.2653 0.0700    1   [7]
2                   nKL
-3.050 -3.000 0.5   xbeginK[0], xendK[0], Kvalue
 0.050  0.012 0.5          [1]       [1]
296.0  0            Tnominal, nT
diaphragm 0
```

```
0  150.0e3          is_burst, P_burst
1  R                left_slug_id, left_slug_end_id
2  L                right_slug_id, right_slug_end_id
slug 0: N2 driver
150  0 0 0.0        nnx, to_end_1, to_end_2, strength
1 0                 viscous, adiabatic
V  0.0              left boundary : velocity (fixed wall)
S  1 L              right boundary: neighbour_slug_id, end
1                   hn_cell
1                   hx_cell
-3.785 -3.015 11 3.25e6 0.0 296.0 Initial: x1, x2, gas, p, u, T
slug 1: N2 test gas
300 0 0 0.0         nnx, to_end_1, to_end_2, strength
1 0                 viscous, adiabatic
S  0 R              left boundary : neighbour_slug_id, end
SD 2 L 0            right boundary: neighbour_slug_id, end, diaphragm_id
1                   hn_cell
1                   hx_cell
-3.015 0.100 11 30.0e3 0.0 296.0 Initial: x1, x2, gas, p, u, T
slug 2: N2 test-section gas
60 0 0 0.0          nnx, to_end_1, to_end_2, strength
1 0                 viscous, adiabatic
SD 1 R 0            left boundary : neighbour_slug_id, end, diaphragm_id
F                   right boundary: free boundary
1                   hn_cell
1                   hx_cell
0.100 0.2653 11 400.0 0.0 296.0 Initial: x1, x2, gas, p, u, T
```

3.4 T4 Shock Tunnel

AIAA-J paper [30].

```
T4 tunnel with M6 nozzle, shot 1098, stage 1.
0                   test_case, dummy value
4 1 2               nslug, npiston, ndiaphragm
214.0e-3   250000   max_time, max_steps
0.5e-6   0.4        dt_init, CFL
2 2                 Xorder, Torder
5.0e-3  1.0e-3      dt_plot, dt_his
6                   hnloc
25.0                hxloc[0], high-pressure end of compression tube
30.0                hxloc[1], shock station 1
32.0                hxloc[2], shock station 2
34.0                     [3], shock station 3
35.9                     [4], nozzle supply region
37.0                     [5], nozzle exit plane
tube definition follows:
```

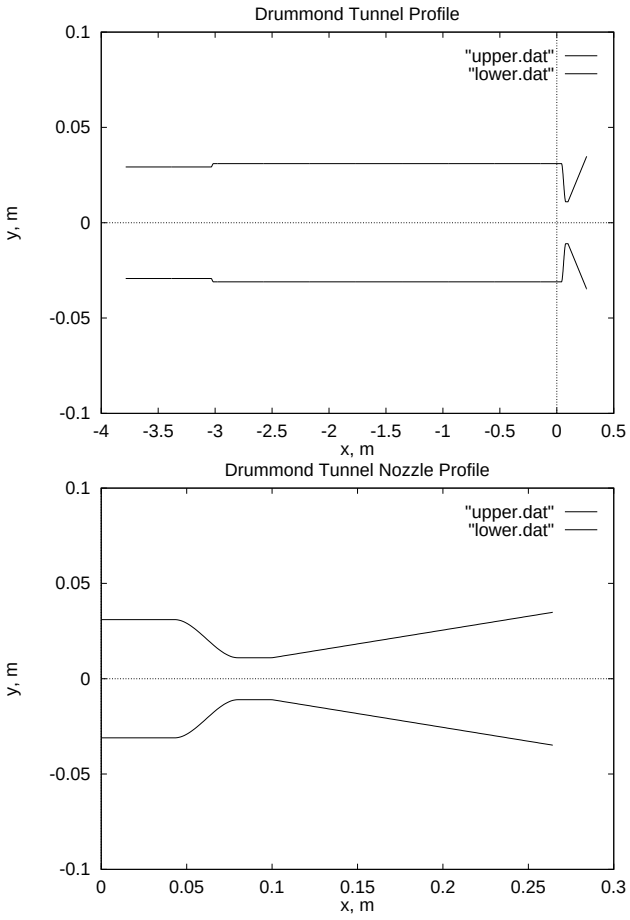

Figure 11: Drummond tunnel cross-section.

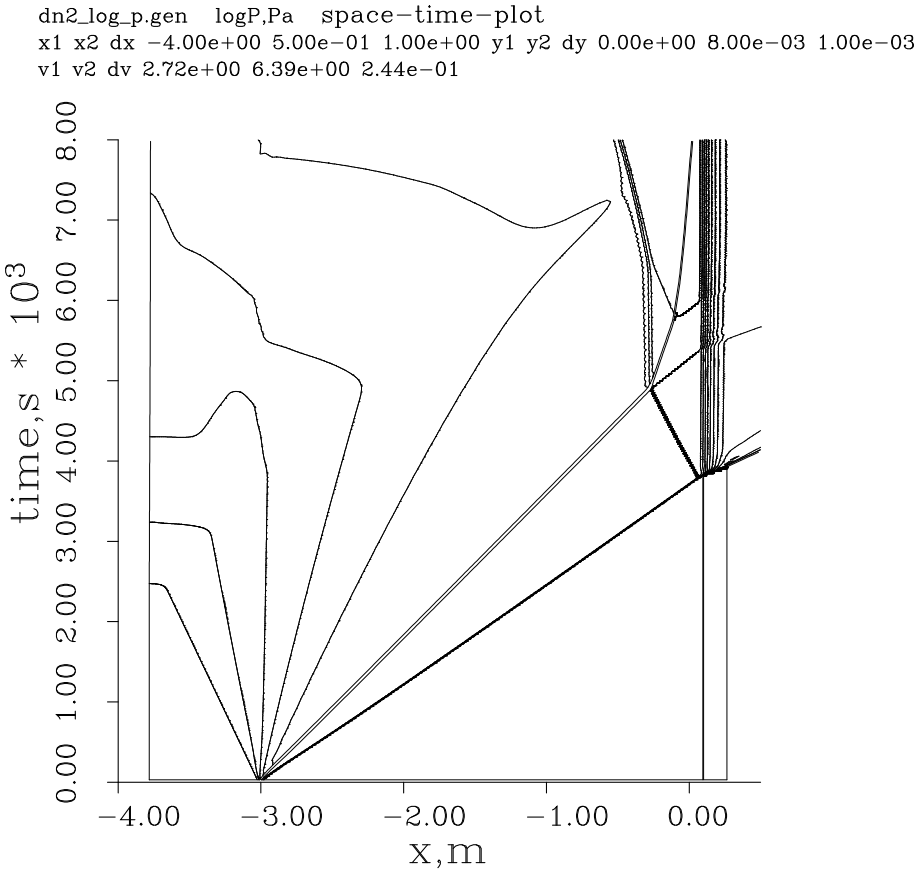

Figure 12: Xt-diagram for Drummond tunnel.

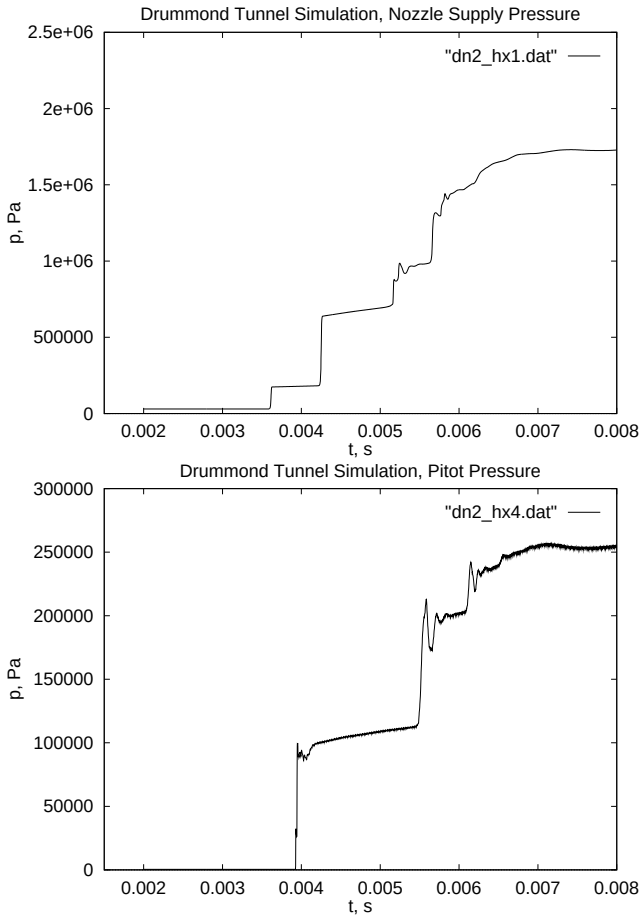

Figure 13: Nozzle-supply pressure and Pitot pressure for Drummond tunnel.

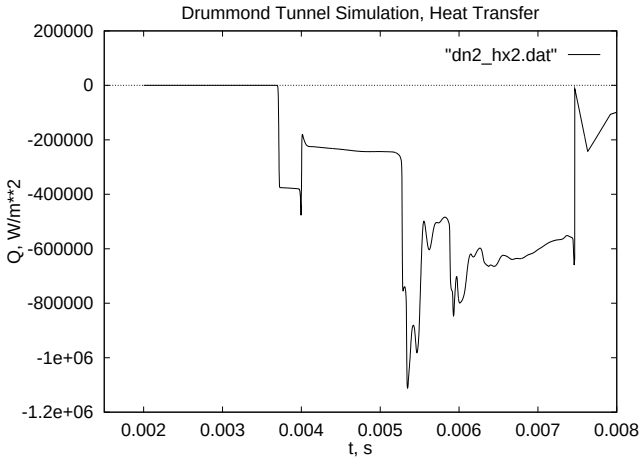

Figure 14: Heat transfer at $x = -0.295$ m for Drummond tunnel.

```
10000  10           n, nseg
-12.30  0.173     0 xb[0], Diamb[0], linear[0]
-1.0    0.173     0   [1]  start contraction to manifold
-0.9    0.168     0   [2]  manifold (equivalent pipe)
-0.1    0.168     0   [3]  start expansion to compression tube
 0.0    0.229     0   [4]  start compression tube
25.9    0.229     0   [5]  start contraction to shock tube
26.0    0.076     0   [6]  start of shock tube
35.9    0.076     0   [7]  start contraction to nozzle throat
36.0    0.025     0   [8]  start parallel nozzle throat
36.05   0.025     0   [9]  start nozzle expansion
37.0    0.262     0   [10] exit plane of nozzle
3                   nKL
-1.0  0.0   0.25    xbeginK[0], xendK[0], Kvalue
26.0  26.1  0.25           [1]       [1]
35.95 36.05 0.25           [2]       [2]
296.0  0            Tnominal, nT
piston [0] is T4 piston with chevron seal
1                       type_of_piston
92.0   0.229  0.470     mass, diam, length
0.0e6   0               p_restrain, is_restrain
25.70   0               x_buffer, hit_buffer
1       0               with_brakes, brakes_on
0       R               left_slug_id, left_slug_end_id
1       L               right_slug_id, right_slug_end_id
0.235 0.0               x0, V0
diaphragm 0
0  57.0e6           is_burst, P_burst
1  R                left_slug_id, left_slug_end_id
2  L                right_slug_id, right_slug_end_id
diaphragm 1
0  600.0e3          is_burst, P_burst
2  R                left_slug_id, left_slug_end_id
3  L                right_slug_id, right_slug_end_id
slug 0: Compressed air to push piston
100  0 1 1.2        nnx, to_end_1, to_end_2, strength
1 0                 viscous, adiabatic
V  0.0              left boundary : velocity (fixed wall)
P  0                right boundary: piston_id
1                   hn_cell
1                   hx_cell
-12.3 0.0 0 4.9e6 0.0 296.0 Initial: x1, x2, gas, p, u, T
slug 1: Helium driver
200  0 0 0.0        nnx, to_end_1, to_end_2, strength
1 0                 viscous, adiabatic
P  0                left boundary : piston
SD 2 L 0            right boundary: neighbour_slug_id, end, diaphragm_id
```

```
1                   hn_cell
1                   hx_cell
0.470 26.0 3 61.6e3 0.0 296.0 Initial: x1, x2, gas, p, u, T
slug 2: Air test gas, in chemical equilibrium
100 0 0 0.0         nnx, to_end_1, to_end_2, strength
1 0                 viscous, adiabatic
SD 1 R 0            left boundary : neighbour_slug_id, end
SD 3 L 1            right boundary: neighbour_slug_id, end, diaphragm_id
1                   hn_cell
1                   hx_cell
26.0 36.0 2 450.0e3 0.0 296.0 Initial: x1, x2, gas, p, u, T
slug 3: Air test-section gas
25 0 0 0.0          nnx, to_end_1, to_end_2, strength
1 0                 viscous, adiabatic
SD 2 R 1            left boundary : neighbour_slug_id, end, diaphragm_id
F                   right boundary: free boundary
1                   hn_cell
1                   hx_cell
36.0 37.0 2 400.0 0.0 296.0 Initial: x1, x2, gas, p, u, T
```

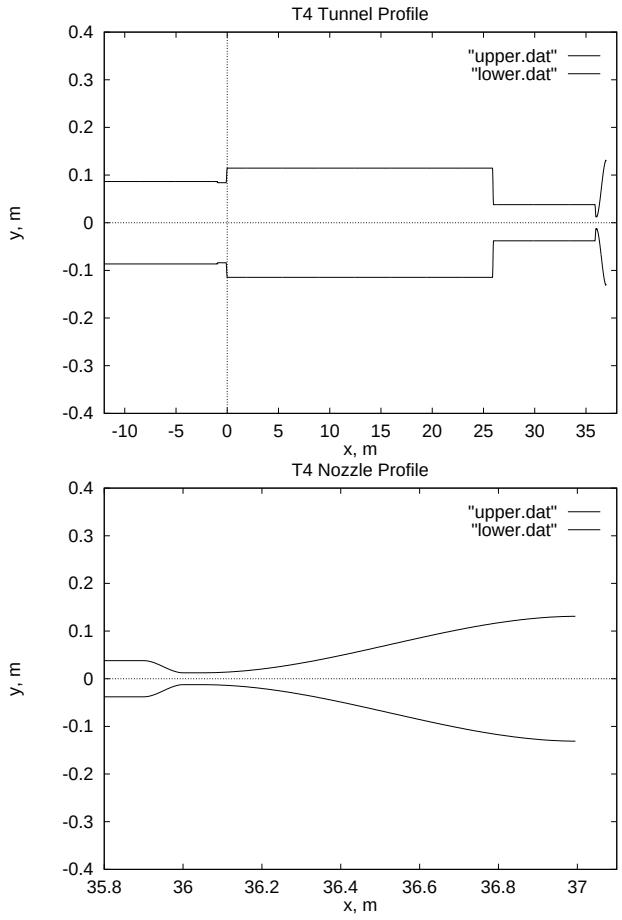

Figure 15: T4 shock tunnel cross-section.

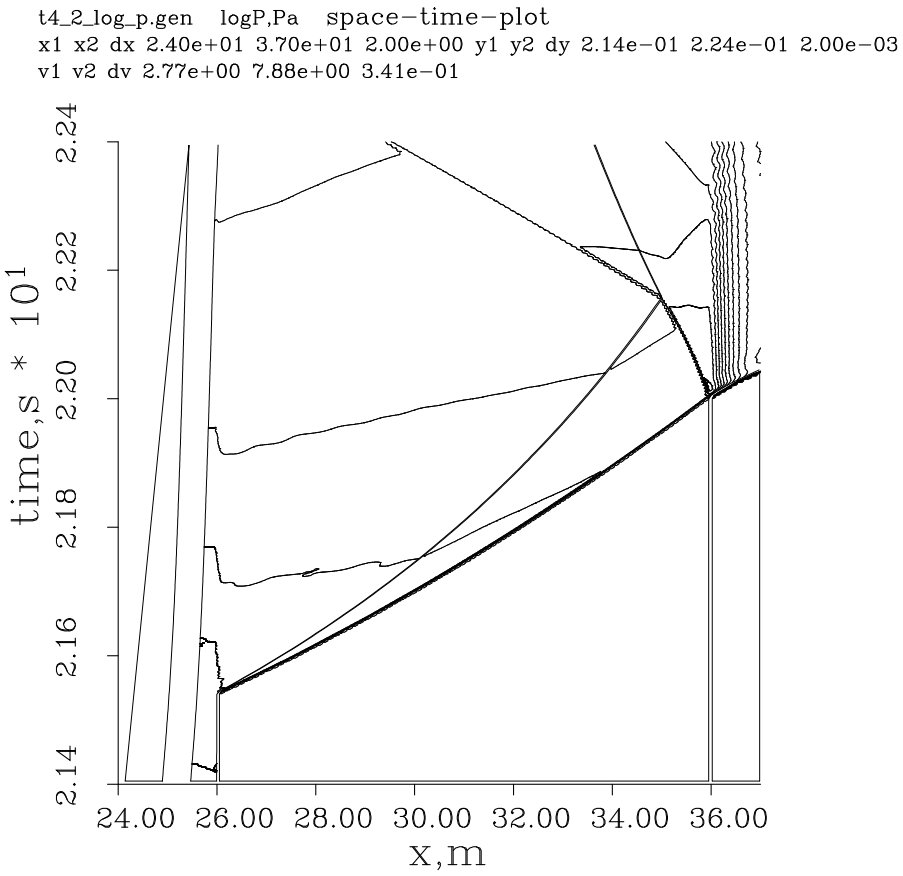

Figure 16: Xt-diagram for T4 shot 1098.

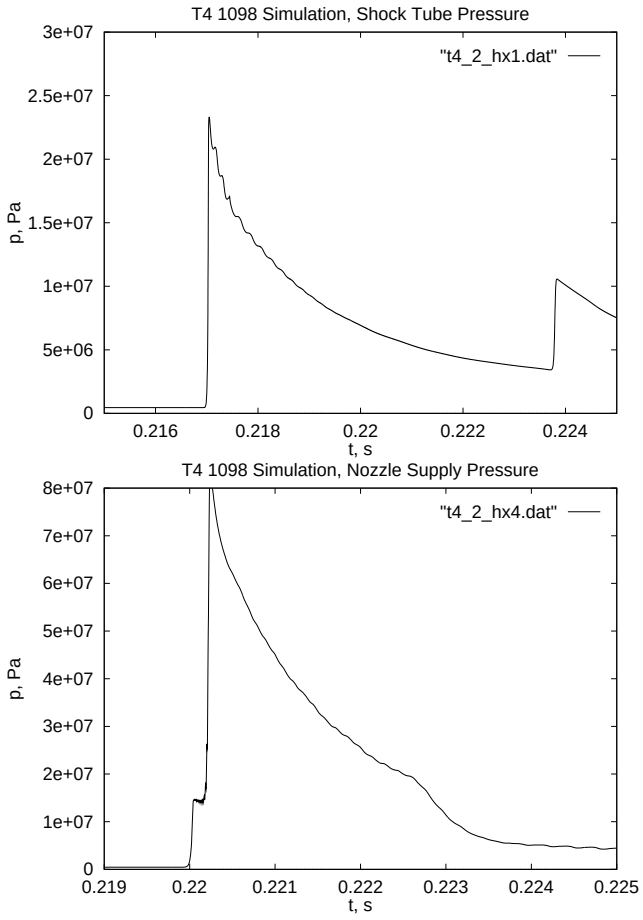

Figure 17: Shock tube and Nozzle-supply pressure for T4 shot 1098.

4 Concluding Remarks

To improve the simulation of contact surface propagation Con Doolan [31] has extended the viscous modelling to include a mass loss from the core folw into the wall boundary layers. This essentially implemented Mirels' analysis [32] on a cell-by-cell basis. It seems to work well for a turbulent boundary layer in that it correctly estimates the test flow duration, however, it doesn't seem to be all that good for laminar flows.

References

[1] H. Bernier and J. Gambart. MOOREA, an internal ballistic code for two stage light gas gun study. In *38th Meeting of the Aeroballistic Range Association.*, 1987.

[2] C. P. T. Groth and J. J. Gottlieb. Numerical study of two-stage light-gas hypervelocity launchers. UTIAS Report 327, Institute for Aerospace Studies, University of Toronto., 1988.

[3] J. Lacey and D. Long. A wave diagram computational method with application to a free-piston shock tube. AIAA Paper 90-1378, 1990.

[4] C. P. T. Groth, J. J. Gottlieb, and P. A. Sullivan. Numerical investigation of high-temperature effects in the UTIAS-RPI hypersonic impulse tunnel. *Canadian Journal of Physics*, 69(7):897–918, 1991.

[5] D. G. Edwards, K. C. Phan, and C. V. Hurdle. Computational modelling of the gas flow from a high-enthalpy blast simulator. In *17th International Symposium on Shock Waves and Shock Tubes*, pages 891–896, 1989.

[6] P. A. Jacobs. L1d: A computer code for the quasi-one-dimensional modelling of transient flow facilities. WBM Internal Report, 1992.

[7] P. A. Jacobs. L1d: a computer program for the simulation of transient-flow facilities. Department of Mechanical Engineering Report 1/99, The University of Queensland, Brisbane, Australia., January 1999.

[8] G. J. Van Wylen and R. E. Sonntag. *Fundamentals of Classical Thermodynamics. 2ed.* Wiley, 1978.

[9] S. Srinivasan, J. C. Tannehill, and K. J. Weilmuenster. Simplified curve fits for the thermodynamic properties of equilibrium air. NASA Reference Publication 1181, 1987.

[10] V. L. Streeter and E. B. Wylie. *Fluid Mechanics.* McGraw-Hill Ryerson, Toronto, 1981.

[11] H. Schlichting. *Boundary-Layer Theory.* McGraw-Hill, New York, 1968.

[12] A. K. Jain. Accurate explicit equation for friction factor. *American Society of Civil Engineers Journal of the Hydraulics Division*, 102(HY5):674–677, 1976.

[13] J. P. Holman. *Heat Transfer.* McGraw Hill, New York, 1981.

[14] H. W. Liepmann and F. E. Goddard. Note on the Mach number effect upon the skin friction of rough surfaces. *Journal of the Aeronautical Sciences*, 24(10):781, 1957.

[15] C. R. Wilke. A viscosity equation for gas mixtures. *Journal of Chemical Physics*, 18:517–519, 1950.

[16] P. K. Sweby. High resolution schemes using flux limiters for hyperbolic conservation laws. *SIAM J. Numer. Anal.*, 21:995–1010, 1984.

[17] P. A. Jacobs. An approximate Riemann solver for hypervelocity flows. *A.I.A.A. Journal*, 30(10):2558–2561, 1992.

[18] S. Osher and F. Solomon. Upwind difference schemes for hyperbolic systems of conservation laws. *Mathematics of Computation*, 38(158):339–374, 1982.

[19] S. K. Godunov (Ed). *Numerical Solution of Multidimensional Problems in Gasdynamics.* Nauka, Moscow, 1976.

[20] J. J. Gottlieb and C. P. T. Groth. Assessment of Riemann solvers for unsteady one-dimensional inviscid flows of perfect gases. *Journal of Computational Physics*, 78(2):437–458, 1988.

[21] H. Gurgenci and W. R. B. Morrison. Rocketdyne shock tunnel: Diaphragm research and development program. WBM Report 6058, 1989.

[22] G. A. Sod. A survey of several finite difference methods for systems of nonlinear hyperbolic conservation laws. *Journal of Computational Physics*, 27(1):1–31, 1978.

[23] C. Hirsch. *Numerical Computation of Internal and External Flows. Volume 2: Computational Methods for Inviscid and Viscous Flows.* John Wiley & Sons, 1990.

[24] M. C. Cline, J. K. Dukowicz, and F. L. Addessio. CAVEAT-GT: A general topology version of the CAVEAT code. Report LA-11812-MS, Los Alamos National Laboratory, 1990.

[25] R. E. Berggren and R. M. Reynolds. The light-gas-gun model launcher. In *Ballistic Range Technology; AGARDograph 138.*, pages 11–94, 1970.

[26] G. O. Roberts. Computational meshes for boundary layer problems. In *Lecture Notes in Physics, 8*, pages 171–177. Springer-Verlag, 1971.

[27] D. A. Anderson, J. C. Tannehill, and R. H. Pletcher. *Computational Fluid Mechanics and Heat Transfer.* Hemisphere Publishing Corporation, New York, 1984.

[28] J. M. Austin, P. A. Jacobs, M. C. Kong, P. Barker, R. Gammie, and B. N. Littleton. The Small Shock Tunnel Facility at UQ. Department of Mechanical Engineering Report 2/97, The University of Queensland, Brisbane, Australia., July 1997.

[29] C. S. Craddock, P. A. Jacobs, and R. Gammie. Operational instructions for the small shock tunnel at uq. Department of Mechanical Engineering Report 8/98, The University of Queensland, Brisbane, Australia., July 1998.

[30] P. A. Jacobs. Quasi-one-dimensional modelling of a free-piston shock tunnel. *A.I.A.A. Journal*, 32(1):137–145, 1994.

[31] C. J. Doolan and P. A. Jacobs. Modeling mass entrainment in a quasi-one-dimensional shock tube code. *A.I.A.A. Journal*, 34(6):1291–1293, 1996.

[32] H. Mirels. Shock tube test time limitation due to turbulent-wall boundary layer. *A.I.A.A. Journal*, 2(1):84–93, 1964.